Brazilian Journal
of Chemical
Engineering

ISSN 0104-6632
Printed in Brazil
www.abeq.org.br/bjche

Vol. 34, No. 02, pp. 583 - 596, April - June, 2017
dx.doi.org/10.1590/0104-6632.20170342s20150500

OIL REMOVAL FROM PRODUCED WATER BY ULTRAFILTRATION USING POLYSULFONE MEMBRANE

S. Kumar[1], B. K. Nandi[2], C. Guria[1] and A. Mandal[1*]

[1]Department of Petroleum Engineering, Indian Institute of Technology (ISM),
Dhanbad 826 004, India.
[2]Department of Fuel & Mineral Engineering, Indian Institute of Technology (ISM),
Dhanbad 826 004, India.
Phone: +91 3262235485. Fax: +91 3262296632
E-mail: mandal_ajay@hotmail.com

(Submitted: June 5, 2015; Revised: February 15, 2016; Accepted: February 21, 2016)

Abstract – The present paper deals with the ultrafiltration (UF) of produced water using a polysulfone membrane. Membranes were prepared by the phase inversion technique using polysulfone (PSf) polymer base, poly vinyl pyrrolidone (PVP) additive and N-methyl-2-pyrrolidone (NMP) solvent. Prepared UF membranes were characterized by determining the surface morphology by scannaing electron microscopy (SEM), atomic force microscopy (AFM), porosity, (iii) water contact angle, equilibrium water content and pure water flux, whereas membrane performance was determined by measuring permeate flux and oil rejection using oily synthetic produced water. With the increase in trans-membrane pressure in the cell, the permeate flux increased significantly, but oil rejection showed a decreasing trend. The best UF membrane performance under different trans-membrane pressures was obtained by maintaining ≥90% oil rejection using an UF membrane with the following composition: PSf- 15%, PVP - 5% and NMP - 80%.

Keywords: Produced water; Polysulfone; Membrane morphology; Porosity; Ultrafiltration.

INTRODUCTION

A large volume of water (called produced water) is usually produced as a byproduct during oil and gas production, which is mixed with dispersed oil, grease, dissolved solids and suspended solids (Chakrabarty et al., 2010). Discharging of produced water may pollute surface and underground water as well as soil. As per environmental regulations the permitted oil and grease limits for treated produced water discharge offshore is 10 $mg.L^{-1}$(Mondal et al., 2008). Typical oil compositions of produced water generated during oil and gas operation are between 100 to 1000 $mg.L^{-1}$ or even higher depending on the oil well and cannot be discharged directly to the environment without treatment (Nandi et al., 2010). Produced water may also be re-injected to some extent into the reservoir for enhanced oil recovery (EOR) after removal of oil and suspended solids to avoid damage to the oil formation (Karhu et al., 2014). Moreover, the direct disposal of produced water to the environment may cause disturbances in ecology. Thus, treatment of produced water before disposal is very important.

Several techniques are available in the literature for the treatment of produced water. In this regard, the gravity settling separation and mechanical coalescence methods are the well known traditional treatment processes. Chemical emulsion breaking is also an effective way to separate oil from produced water (Karhu et al., 2014). The coagulation and air flotation (Wei et al., 2013, Mandal et al., 2003),

*To whom correspondence should be addressed

electrostatic and electrocoagulation separation methods were also applied to separate oil and water from produced water (Sarkar and De, 2011). However, these methods would lead to a huge production of sludge with complicated operational problems. Microwave treatment (Sahoo and De, 2010) and heat treatment (Chen and He, 2003) have been occasionally applied to oily water treatment in recent years. But all these methods are very complicated and it takes more time to separate oil from produced water (Karhu et al., 2014; Wei et al., 2013; Sarkar and De, 2011; Sahoo and De, 2010; Chen and He, 2003; Kumar et al., 2015) All these methods are not efficient when the oil concentration is below 400 $mg.L^{-1}$ and the oil droplet size is less than one micrometer (Padaki et al., 2015).

Under such circumstances, the use of membranes offers a potential solution to the problem of oily produced water purification. The porous membrane matrix can promote coalescence of micron and submicron oil droplets into larger ones that can be easily separated by gravity. Common membrane separation techniques employed for the separation of oil from oily wastewater are: (i) microfiltration (Nandi et al., 2010), (ii) pervaporation (Mohammadi et al., 2003; Hlavacek, 1995), (iii) electrocoagulation (Ghosh et al., 2010), (iv) reverse osmosis (Duong and Chung, 2014; Mahendran et al., 2004) and (v) ultrafiltration (Nandi et al., 2009; Sarkar and De, 2010; Singh et al., 2011). However, few studies addressed the application of polysulfone (PSf) membranes in wastewater treatment. Sinha and Purkait (2013) tested a hydrophilic ultrafiltration (UF) polysulfone membrane in cross flow mode to treat oil field produced water. Bhattacharjee et al. (1992) studied a tubular UF model equipped with polyvinylidenefluoride membranes modified by inorganic nano-sized aluminum particles to treat oilfield-produced water. Vatanpour et al. (2011) used poly(vinyl pyrrolidone) (PVP) as additive on poly(ether sulfone) (PES) membranes and showed that addition of PVP increased the pure water flux. Chakrabarty et al. (2010) reported the effect of different molecular weight of polyethylene glycol (PEG) on the morphology and performance of PSf membranes prepared with N-methyl-2-pyrrolidone (NMP) and dimethyl acetate (DMAc) as a solvent separately and found that the molecular weight of PEG played a significant role on the morphology and properties of the membranes prepared. Polysulfone membranes for separation of oily water were used because they has the following advantages: (i) highly resistant to mineral acids, alkali, and electrolytes, in pH ranging from 2 to 13, (ii) resistant to oxidizing agents, therefore they can be cleaned by bleaches (iii) resistant to surfactants and hydrocarbon oils, (iv) soluble in solvents like DMAc and NMP, making it easily applicable for the conventional phase inversion processes (v) good mechanical strength and permeability (vi) ability to modify the properties through blending with other polymers.

In this paper, we reported the use of polysulfone based membrane for the separation of oil from oily produced water with varying oil concentration (< 400 $mg.L^{-1}$) to meet the environmental requirements. The surface morphology of the membrane was analyzed by Field Emission Scanning Electron Microscopy (FE-SEM), Atomic Force Microscopy (AFM), pore size distribution, Porosity and pure water flux. The oil droplet size distribution of produced water was measured to evaluate the membrane performance. The effects of trans-membrane pressure (TMP), oil concentration and oil droplet size in the feed on the permeate flux and oil removal efficiency were studied.

EXPERIMENTAL

Materials

Polysulfone (MW. 75,000 Da) was supplied by Sigma-Aldrich Co, USA and was used as the main polymer in the membrane casting solution. Reagent grade N-methyl-2-pyrrolidone (99.5% purity) was supplied by Central Drug House Ltd., India, and poly(vinyl pyrrolidone) (MW. 40,000 Da) was supplied by LobaChemie Ltd, India. Crude oil was collected from the Digboi area (Oil India Limited, India) and synthetic produced water was prepared using this crude oil. The properties of crude oil, which were determined experimentally, are given in Table 1. The distilled water was used to prepare synthetic produced water (SPW). Tetrachloroethylene with purity > 99.9 % (wt/wt) was used as a solvent to measure the oil content in SPW and supplied by Beker (USA).

Table 1. Compositions and characteristics of crude oil

Sl. No.	Parameters	Values
1	Density (15.5 °C) ($kg.m^{-3}$)	855.60 ± 10
4	Viscosity (cp) at 30°C	525 ± 10
5	Acid Number (mg KOH/g)	0.038 ± 0.002
6	Pour Point (°C)	18 ± 0.5
7	Saturates (%wt/wt)	55 ± 2
8	Aromatics (%wt/wt)	35± 1
9	Resins (%wt/wt)	7.9± 0.1
10	Asphaltenes (%wt/wt)	1.2± 0.1

Preparation of synthetic produced water

Synthetic produced water (SPW) was prepared using crude oil (properties of crude oil are given in Table: 1) procured from the Digboi oil field, Assam, as a dispersed phase and distilled water as a continuous phase. The measured amount of crude oil and distilled water was taken in a beaker and kept in a sonicator water bath (FB15051, Fisherbrand, Germany) for about 5-10 hrs depending upon the oil concentration at a temperature of 27°C. The

resulting o/w emulsion showed a uniform yellowish colour. The average size and the size distribution of oil drops were estimated with a Zetasizer (Model: Nano-S90, Make: Malvern Instruments Ltd., UK). An optical microscope (Model: BX51, Make: Olympus, Japan) was used to observe the morphology of the SPW. The images were acquired by digital image extracting equipment attached to the microscope. The total oil and grease (TOG) in SPW was measured with a TPH/TOG analyzer (Model CVH, Make: Wilks Enterprise). The total dissolved solids (TDS), salinity and pH of SPW were also measured by a multi parameter tester (Model: PCSTestr 35, Make: Singapore). The details properties of prepared SPW are shown in Table 2.

Table 2. Properties of SPW used in the experiments at a temperature of 27°C

Type of produced water	pH, ± 0.1	Oil content ($mg.L^{-1}$)	TDS (ppm), ± 1	Salinity ($mg.L^{-1}$),± 1	Average Oil droplet size (nm),± 10
E_{100}	8.87	100	11	16	502
E_{200}	8.57	200	14	19	514
E_{300}	8.70	300	25	26	751
E_{400}	8.20	400	33	34	938

Membrane preparation

The membrane casting solution was prepared by blending an appropriate composition of polysulfone, NMP solvent and PVP additive under constant stirring using a magnetic stirrer at 50°C for 6.0 hrs. A series of casting solutions was prepared and allowed to stand for 4.0 hours to remove air bubbles. After removing air bubbles, the casting solution was cast onto a clean glass plate and spread uniformly at a fixed rate, keeping the desired gap (100 μm) between glass plates and metal rod at 27°C. After casting, the casted film, along with the glass plate, was immersed horizontally into a distilled water bath at a temperature of 27°C for 24.0 hours to remove the residual solvent and to solidify the membrane. The phase immersion precipitation occurs when the casting film along with the glass plate is immersed into water. In the phase inversion process, the formation of membrane pores is controlled by both the thermodynamics of the casting solution and the kinetics of the transport process. The thermodynamics of the casting solution are related to the phase equilibrium between the components of the casting solution, while the kinetics of the transport process can be described by the mutual diffusion and transport of the components. In the phase inversion processes, a liquid polymer solution is precipitated into two phases, i.e., a polymer-rich phase that will form the matrix of the membrane and a depleted polymer phase that will form the membrane pore in the membrane structure. The porous membrane morphology is then fixed according to the subsequent solidification process. Finally, the prepared membranes were stored in distilled water until the ultrafiltration experiments. Three different membranes under varying composition of PSf and PVP were prepared with fixed thickness of 100 micrometer, which were designated as M_1, M_2, M_3; details are given in Table 3. The prepared membranes were characterized by morphological analysis using FE-SEM (Model: Supra 55, Make: Carl Zeiss, Germany) and AFM analysis. AFM analysis were performed using a Dimension Icon (Nano Scope V, Bruker, USA) in Scan Asyst contact and taping mode**.** All the images were processed using the same Instrument (Dimension Icon) attached software. The software directly provides the values for the mean roughness.

Table 3. Composition of membrane casting solutions and corresponding dry membranes

Membrane casting solutions (wt %)				Dry membrane (wt%)	
Membrane	PSf	PVP	NMP	PSf	PVP
M_1	10	5	85	66.67	33.33
M_2	12	5	83	70.58	29.42
M_3	15	5	80	75.00	25.00

Experimental apparatus and procedure

The membrane cell (capacity 500 ml, material of construction SS-316) was used to carry out the stirred batch experiments with the flat circular membrane of diameter 0.068 m with effective area 3.631×10^{-3} m^2. A typical ultra-filtration setup is shown in Fig. 1. The cell was pressurized using nitrogen gas. The permeating solution was collected from the bottom of the cell. Before using a fresh membrane, it was compacted with de-ionized water for 4 hours at a transmembrane pressure of 450 kPa which is higher than the maximum operating pressure in the present study.

Pore size distributions of membranes were measured from SEM images using the 'ImageJ Launcher Broken Symmetry Software package' under the assumption that the shapes of the pores are circular.

A hydrophilic membrane surface is beneficial to antifouling and permeation performance of the membrane. In general, the hydrophilicity is evaluated by the contact angle between membrane and water. The water contact angle of membranes is influenced by surface roughness, porosity, and types of additive in the membrane. To enhance the hydrophilicity of PSf membrane, poly(vinyl

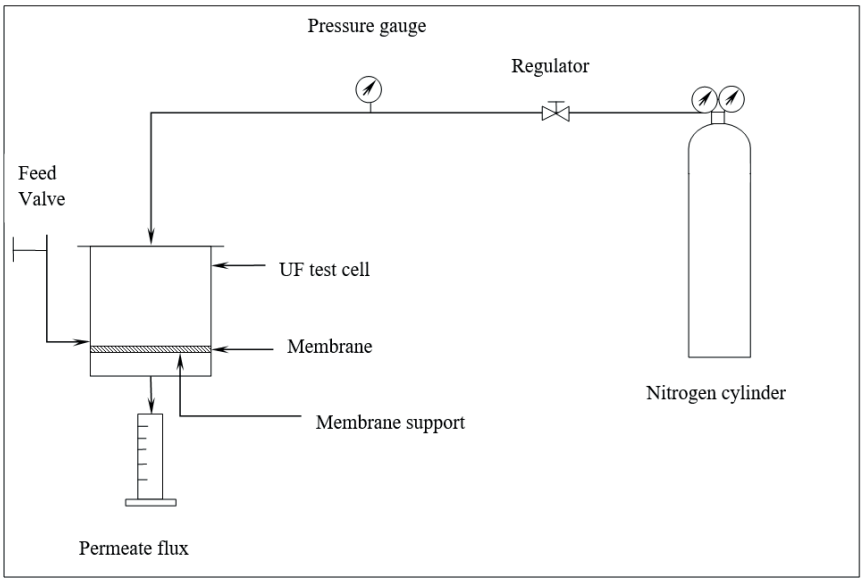

Figure 1. Experimental set-up for separation of oil from produced water.

pyrrolidone) (PVP) additive was used in the membrane preparation. The contact angle between water and membrane was measured using a contact angle goniometer (Drop shape Analyzer DSA25, Kruss, Germany) at a temperature of 27°C to evaluate membrane hydrophilicity. For this, accurately measured 10 µL of water was put on the membrane surface with an automatic piston syringe and photographed. To minimize the experimental errors, the contact angle of each membrane was measured five times and the average value is reported.

Membrane porosity (φ) is a measure of permeate holding capacity of the membrane and it was measured by a gravimetric method. The dried membrane samples were weighed and then immersed into octane in order to fill the pores. Porosity, φ (%), was calculated as the quotient of the volume of pores (V_{pore}) and the total volume of the dry membrane.

$$\varphi = \frac{V_{pore}}{V_{membrane}} \times 100 \tag{1}$$

The volume occupied by the pores, (V_{pore}) was deduced from the weight difference between dry membrane (M_{dry}) and wet membrane (M_{wet}) sample, $V_{pore} = \frac{M_{wet} - M_{dry}}{\rho_{octane}}$, where the density of octane (ρ_{octane}) is 0.79 g/cm^3.

Equilibrium water content (*EWC*) is indirectly related to the porosity and degree of hydrophilicity of the membranes and calculated by the following equation.

$$EWC = \frac{w_0 - w_1}{w_1} \times 100 \tag{2}$$

where W_0 = wet sample weight (kg), W_1 = dry sample weight (kg).

The water flux was calculated from the experimental permeate flow rate measured at every 5 min interval after attaining flow stabilization.

Distilled water and produced water permeate fluxes were measured using different membranes after compaction at different trans-membrane pressure using a standard flux equation.

$$J_p = \frac{V_p}{A\Delta t} \tag{3}$$

where J_p = permeate flux, V_p= volume of permeate, A= area of the membrane and Δt = time taken to collect the measured amount of permeate collected at different transmembrane pressures.

Percentage Oil rejection was calculated by the following equation.

$$R(\%) = \left(1 - \frac{C_p}{C_f}\right) \times 100 \tag{4}$$

where c_p is the oil concentration in the permeate and c_f is the oil concentration in feed.

RESULTS AND DISCUSSION

Droplet size distribution and morphology of the SPW

The droplet size distributions of the SPW with different oil concentrations are given in Fig. 2. The droplet sizes of all these SPW show a normalized distribution with average oil droplet sizes in the range from 502-938 nm depending on the concentration of crude oil in the SPW.

The microscopic images of SPW are shown in Fig. 3. From Fig. 3 it can seen that the oil droplets are in dispersed form, whereas water is continuous. Fig. 3 is obtained

during microscopic analysis, in which oil droplets rest on a glass slide and deformed easily. Therefore, reported oil droplet size is greater than the actual size. In contrast, oil droplet size in Fig. 2 was obtained using a Zetasizer analyzer, where oil droplets were in suspension, giving a more accurate measurement of oil droplet size distribution. As the concentration of dispersed phase, i.e., oil phase increased, the frequency of droplet collisions during agitation increased, resulting in the merger of smaller oil droplets to form bigger droplets.

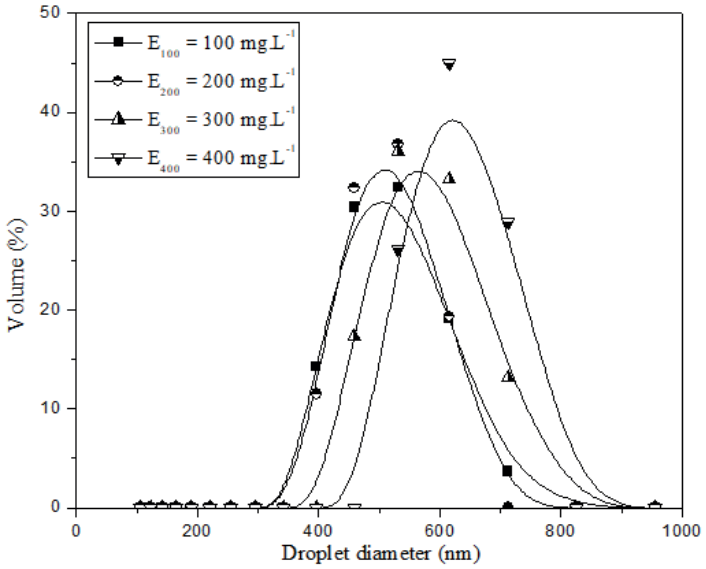

Figure 2. Droplet size distributions of SPW with different oil concentration.

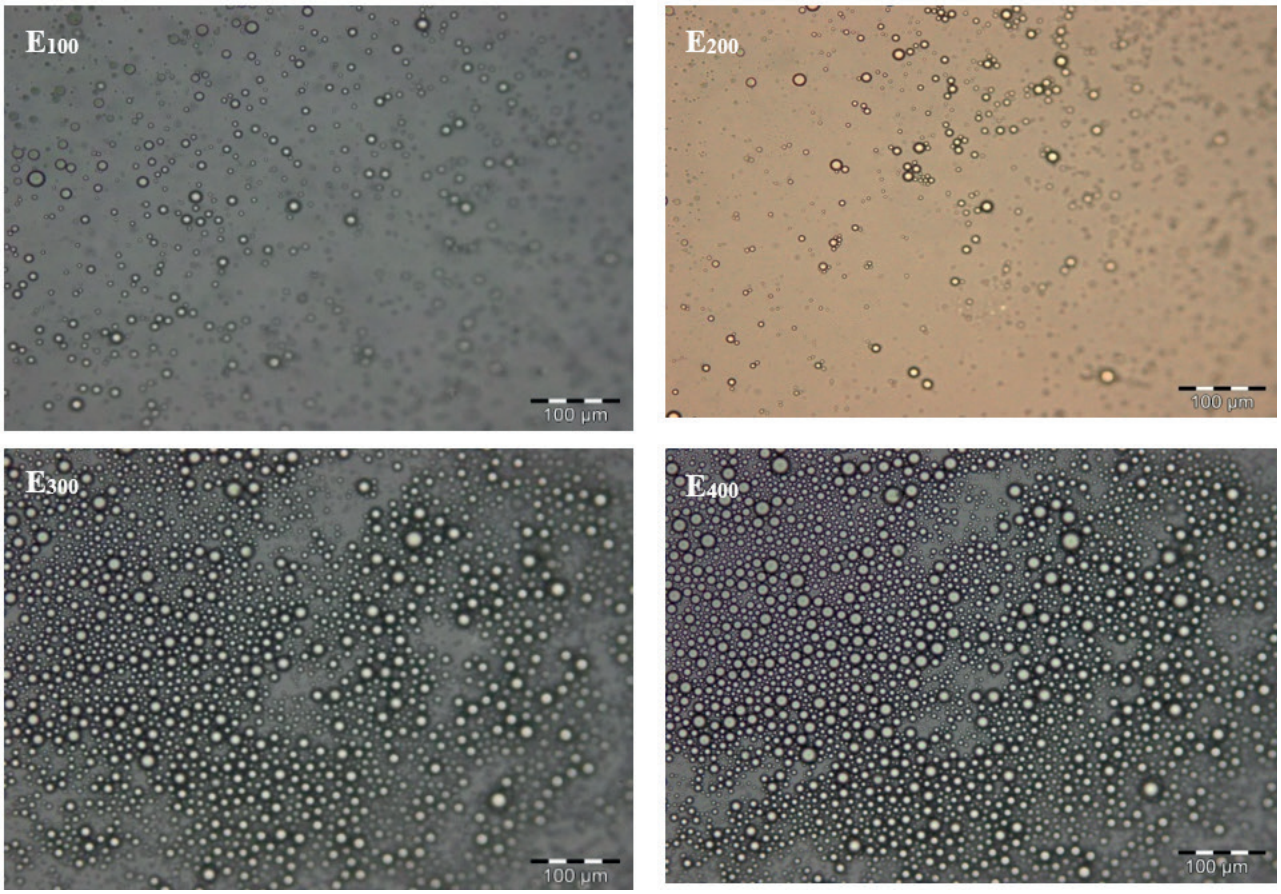

Figure 3. Optical microscopic images of synthetic produced water, E_{100}: 100 mg.L^{-1}, E_{200}: 200 mg.L^{-1}, E_{300}: 300 mg.L^{-1}, E_{400}: 400 mg.L^{-1}.

Characterization of membranes

Scanning electron microscopic analysis

Fig. 4A shows the top surface and Fig. 4B shows the cross-sectional FE-SEM images of different membranes. It can be seen from Fig. 4B that the membranes have an asymmetric structure and porous sub layer. The sub layer seems to have finger – like pores as well as macro void structures. From Fig. 4A it is found that the surface pore size decreased slightly when the PSf composition increased from 10 % to 15%. However, the pore size, which appears on the surface is not an effective pore of the membrane because pores have a tortuous pattern and therefore the effective pore size is nuch smaller than the surface pore size. Fig. 4B shows the tortuous pattern of membrane pores. All the membranes have dense top skin layers, a porous sub-layer and sponge-like bottom layer. These structures are formed due to the high mutual affinity of NMP for water, resulting in instantaneous demixing.

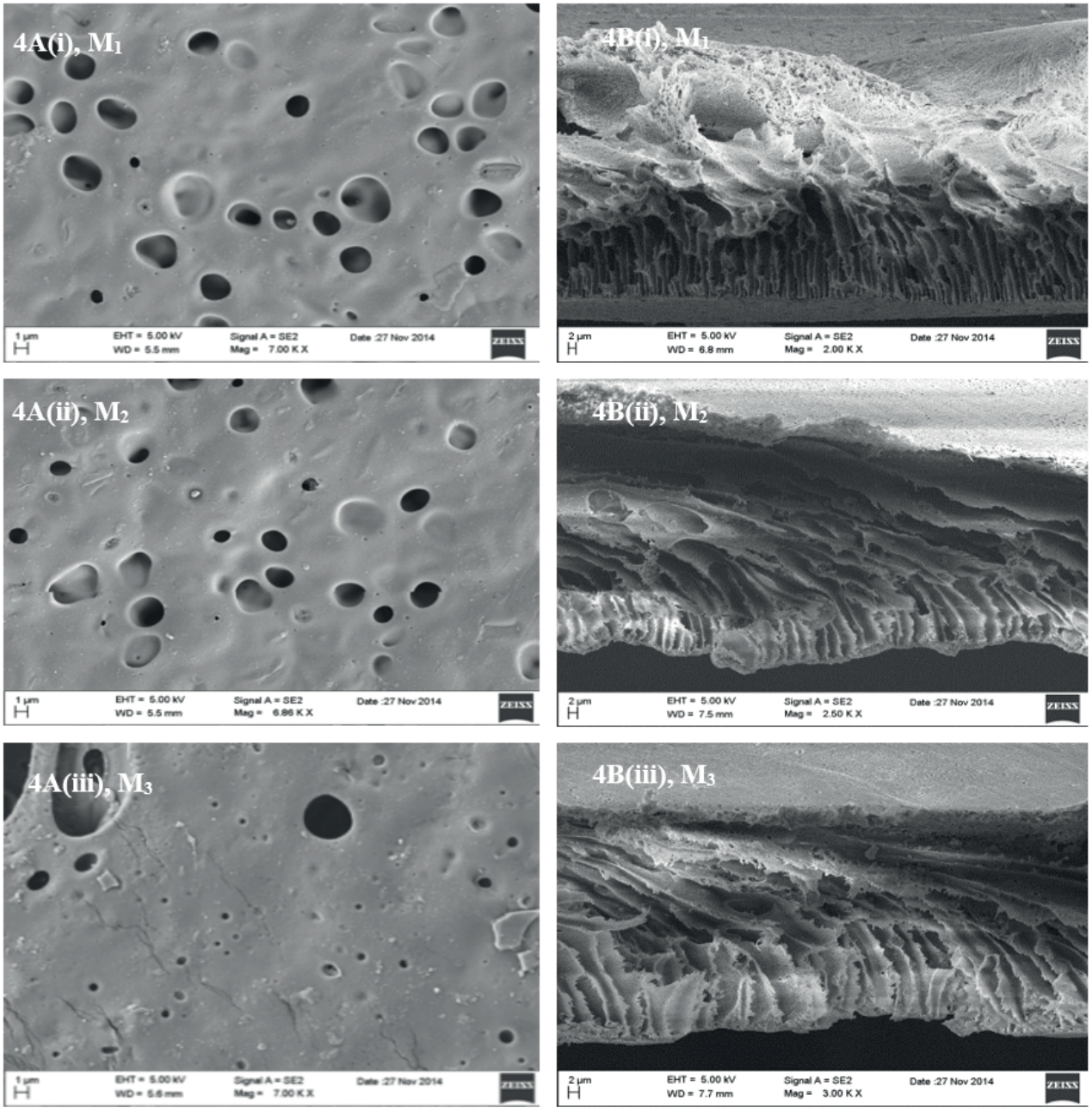

Figure 4. 4A. To-surface FE-SEM images of membranes (i) M_1 (PSf: 10%), (ii) M_2 (PSf: 12%) and (iii) M_3 (PSf: 15%). **4B**. Cross-sectional FE-SEM images of membranes (i) M_1 (PSf: 10%), (ii) M_2 (PSf: 12%) and (iii) M_3 (PSf: 15%).

AFM analysis of membrane

Fig.5A: shows the height sensor AFM image of membranes M_1, M_2, M_3 and Fig. 5B shows the pore dimension of the corresponding membranes. Fig. 5B(i) shows that the pore size of membrane M_1 lies around 270 nm, whereas the depth of the pore is in the range of 91 nm. Fig. 5B (ii) shows that the pore size of membrane M_2 lies around 200 nm, whereas the depth of the pore is in the range of 50 nm. Similarly the pore size of membrane M_3 lies around 150 nm and the depth of the pore in the range of 40 nm.

Pore size distribution

Pore size distributions of identical membrane areas for each type of membrane are shown in Fig. 6. From Fig. 6 it is observed that, with increase in polymer (PSf) concentration, the pore size of the corresponding membranes decreases and the pore size distribution becomes narrower. The pore sizes

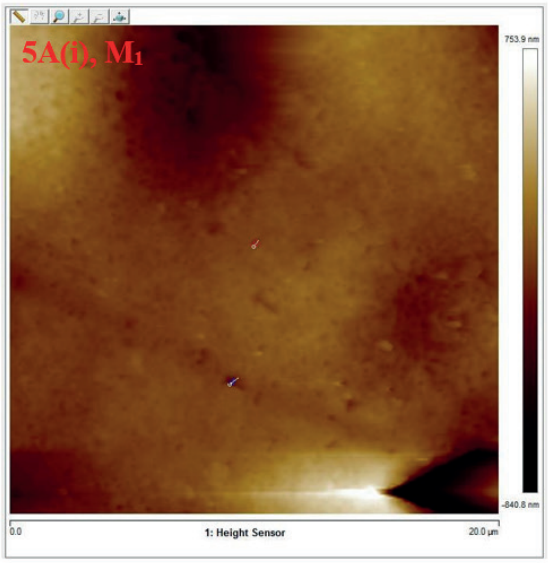

5B(i), M_1

Pair	Horizontal Distance	Vertical Distance	Surface Distance	Angle	Rmax	Rz	Rz Count	Rms	Ra (Frequency Cutoff)	Frequency Cutoff	Radius	Radius Sigma
1	0.083 (µm)	59.502 (nm)	0.103 (µm)	35.575 (°)	16.150 (nm)	0.000 (nm)	0.000	19.909 (nm)	5.593 (nm)	6.010 (µm)	0.270 (µm)	0.616 (nm)
2	0.091 (µm)	-48.003 (nm)	0.106 (µm)	-27.691 (°)	10.579 (nm)	10.579 (nm)	2.000	17.703 (nm)	3.459 (nm)	0.000 (µm)	0.070 (µm)	0.008 (µm)

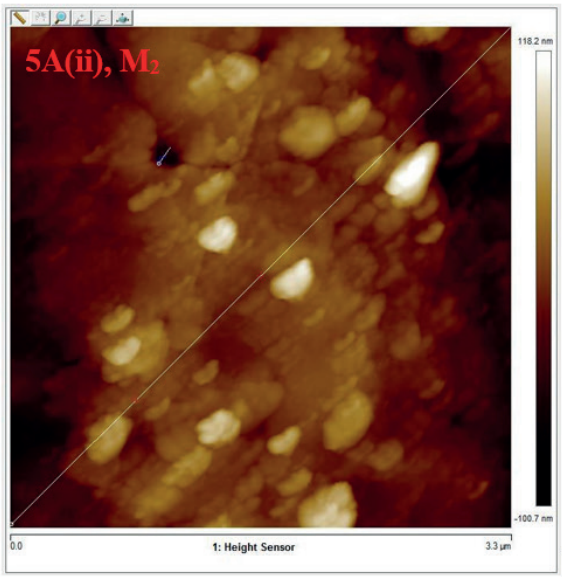

5B(ii)M_2

Pair	Horizontal Distance	Vertical Distance	Surface Distance	Angle	Rmax	Rz	Rz Count	Rms	Ra (Frequency Cutoff)	Frequency Cutoff	Radius	Radius Sigma
1	0.076 (µm)	-171.707 (nm)	0.206 (µm)	-66.082 (°)	187.276 (nm)	0.000 (nm)	0.000	61.439 (nm)	40.807 (nm)	0.000 (µm)	0.143 (µm)	0.004 (µm)
2	0.270 (µm)	-4.752 (nm)	0.478 (µm)	-1.007 (°)	160.640 (nm)	157.820 (nm)	2.000	42.422 (nm)	31.019 (nm)	0.000 (µm)	0.128 (µm)	0.011 (µm)

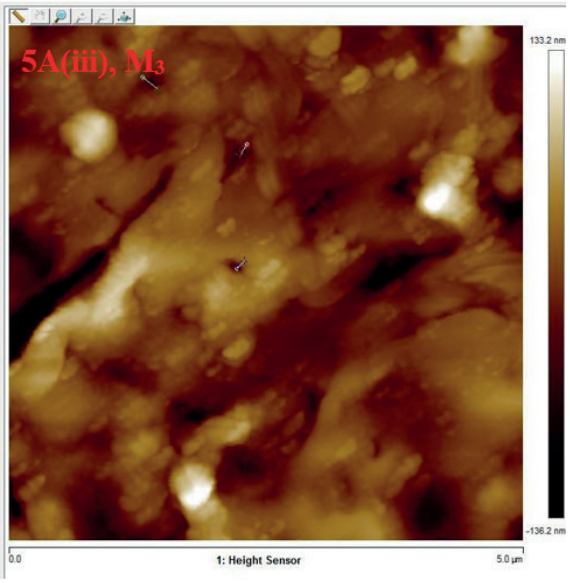

5B(iii)M3

Pair	Horizontal Distance	Vertical Distance	Surface Distance	Angle	Rmax	Rz	Rz Count	Rms	Ra (Frequency Cutoff)	Frequency Cutoff	Radius	Radius Sigma
1	0.201 (µm)	-15.936 (nm)	0.208 (µm)	-4.536 (°)	35.909 (nm)	0.000 (nm)	0.000	38.706 (nm)	24.055 (nm)	0.000 (µm)	0.204 (µm)	0.000 (nm)
2	0.088 (µm)	-27.471 (nm)	0.092 (µm)	-17.395 (°)	16.373 (nm)	0.000 (nm)	0.000	0.000 (nm)	8.186 (nm)	1.901 (µm)	1.565 (µm)	0.726 (nm)

Figure 5. AFM image and pore dimensionS of membranes M_1, M_2 and M_3.

of the prepared membrane lie in the range of ultrafiltration. The pore size of membrane $M_1$is 0.3 µm, whereas for membrane M_3 the pore size is 0.17 µm. Therefore, through membrane M_3 the water flux and oil rejection are greater compared to the other two membranes.

The pore size decreased due to the increase in polymer (PSf) concentration and the corresponding decrease in wt.% of PVP (on dry basis) in the membrane matrix. As the UF membrane was prepared by the phase inversion technique, the dry membrane consists of PSf and PVP, excluding NMP solvent. Therefore, the weight percent of PVP in the dry membrane will decrease with the increase of PSf.

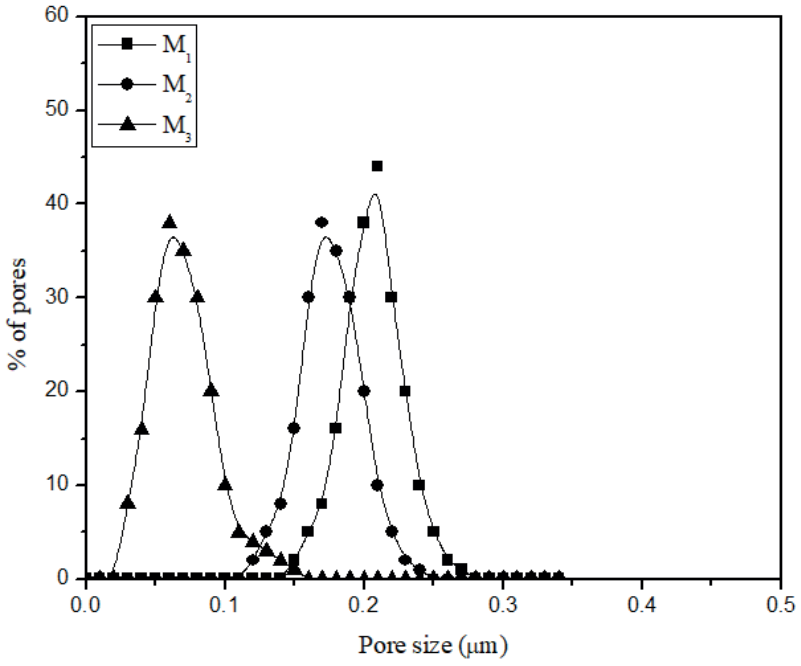

Figure 6. Pore size distribution of membranes M_1 (PSf: 10%), M_2 (PSf: 12%) and M_3 (PSf: 15%).

Membrane hydrophilicity

Fig. 7 shows the variation of water contact angle with polymer (PSf) loading in the membranes**.** As shown in Fig. 7, the increased loading of polymer causes an increase in the contact angle (60 to 75°). This is due to increased PSf concentration in the membrane, resulting in a decrease in hydrophilic additive (PVP) concentration in the membrane matrix. A distinct decrease in water contact angle (by 20 %) was observed for M_1 (PSf: 10%) membrane over M_3 (PSf: 15%) membrane. The reduction of water contact angle is a direct indication of improved hydrophilicity of the PSf-PVP membrane.

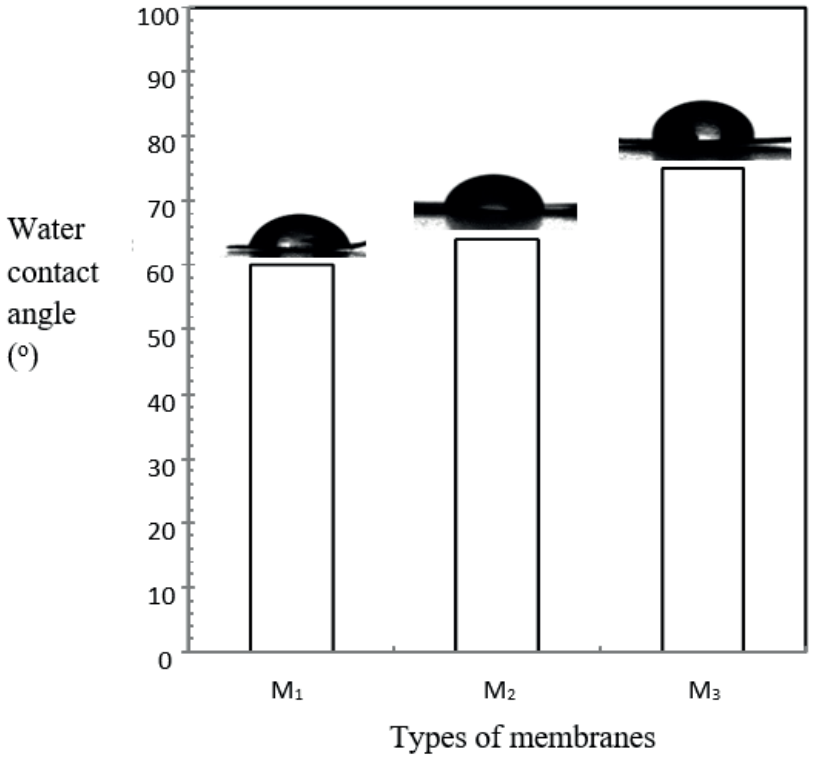

Figure 7. Variation in water contact angle of the different membranes M_1 (PSf: 10%), M_2 (PSf: 12%) and M_3 (PSf: 15%).

Performance of membranes

Permeate flux

Variation of the permeate flux with pressure is shown in Figs. 8a-8c, using three different membranes (Table 3). It was found that the distilled water flux is higher than producing water at a given trans-membrane pressure drop for all types of membranes. This is because in distilled water there are no dispersed particles (oil droplets) which may block the pores of the membranes. In a pressure-driven process there are various types of membrane resistances (for example, pore blocking, adsorption, membrane resistance, gel layer resistance, concentration polarization, etc). But in the case of pure water flux, membrane resistance depends only on the pore structures of the membrane. As the transmembrane pressure (TMP) increased during filtration, the pore structures of the membranes were compacted, which resulted in a decrease in the void fraction. As the decrease in void fraction is non-linear with pressure, the resulting pure water flux is also non-linear with TMP. The increase in the flux with an increase in TMP is due to the increase in driving force (Δp). Therefore, higher flux is obtained at higher TMP for all the membranes. The permeate flux data were taken under steady-state conditions under constant stirring. Constant stirring at 500 rpm will help to attain constant flux with reduced gel polarization condition. From all three figures (Figs. 8a - 8c) it is seen that, of all the three membranes, the highest flux, 86 $L.m^{-2}.h^{-1}$, was obtained for E_1 feed through M_1 membrane at a TMP of 400 kPa and the lowest flux, 11 $L.m^{-2}.h^{-1}$, of E_4 was obtained through M_3 at a TMP of 100 kPa. For distilled water the permeate flux gradually increased with TMP and at 100 kPa flux was 79 $L.m^{-2}.h^{-1}$, whereas at 400 kPa the flux was 252 $L.m^{-2}.h^{-1}$. From these figures, it is seen that the permeate flux of E_1 through membrane M_1 is more than that through the M_3 membrane, since the pore size and number of pores in membrane M_3 are lower than in M_1. Similar trends were

also observed for SPW E_{200}, E_{300} and E_{400}. The pure water flux, equilibrium water content and porosity are given in Table 4. From Table 4, it is observed that, when the PSf composition increased from 10 % to 15 %, the pure water flux (PWF) decreased from 90 $L.m^{-2}.h^{-1}$ to 72 $L.m^{-2}.h^{-1}$; similarly, the equilibrium water content (EWC) decreased from 34.62% to 16% and porosity decreased from 0.37 to 0.20. These results indicate that the prepared membranes became less porous when the PSf composition increased.

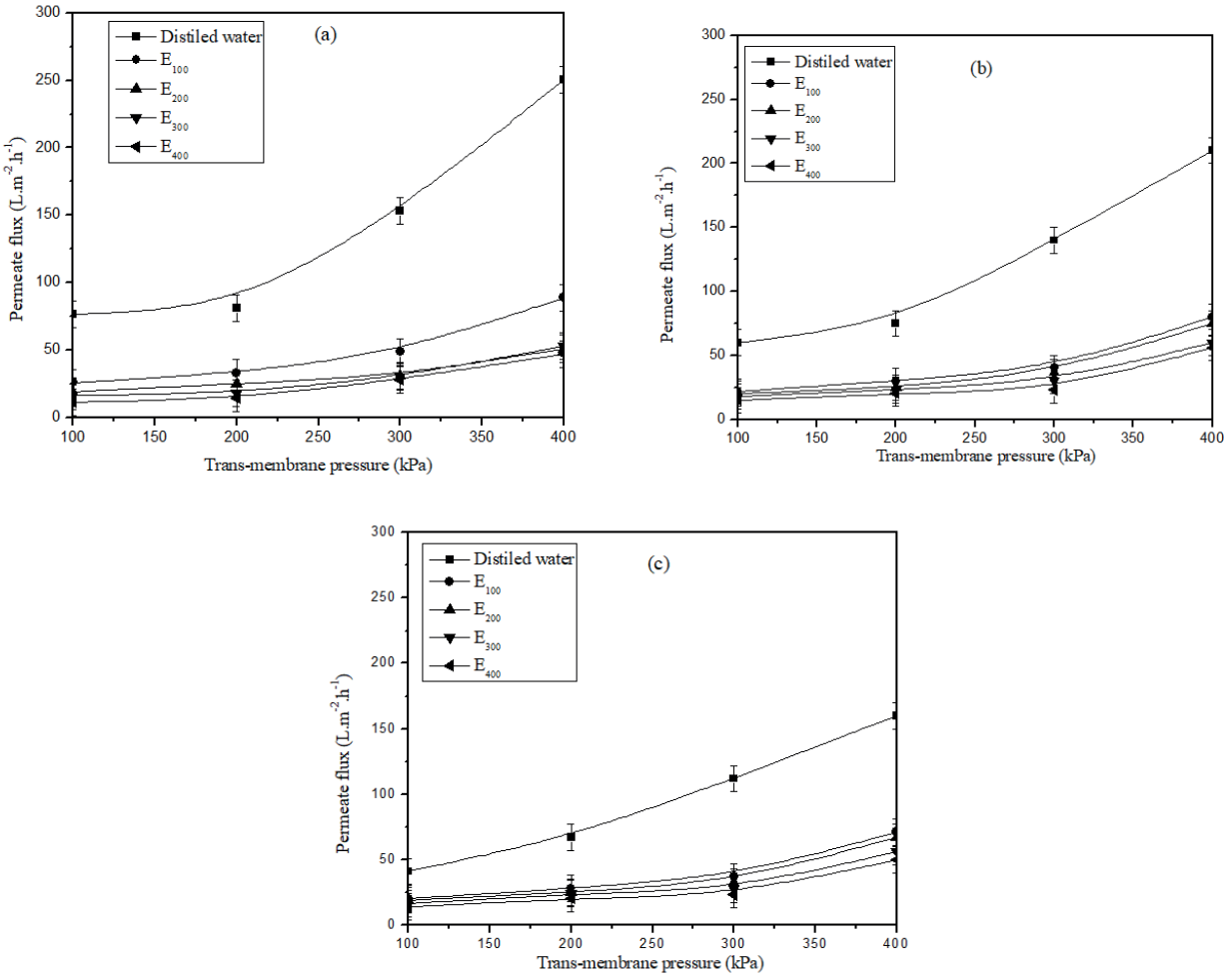

Figure 8. Permeate flux of distilled water and synthetic produced water through membranes M_1 (PSf: 10%), M_2 (PSf: 12%) and M_3 (PSf: 15%).

Table 4. Properties of the membranes used for the experiment

Membranes	Pure water flux (PWF, $L.m^2.h^{-1}$) at 100 kPa, ± 5	Equilibrium water content (EWC, %), ± 1	Porosity (φ), ± 0.1
M_1	90	34	0.37
M_2	79	18	0.27
M_3	72	16	0.20

Oil concentration in the permeate

Variation of the oil concentration in the permeate flux with TMP and initial oil concentration in the feed is shown in Figs. 9a-9d. From Fig. 9a it may be seen that the oil concentration in the permeate increased with an increase in TMP. This is due to the fact that, at higher TMP, some oil droplets penetrate the porous membranes. At a particular TMP the oil concentration in the permeate is higher for membranes with higher porosity. At 100 kPa

the oil concentrations in the permeate were 21 mg.L^{-1}, 18 mg.L^{-1} and 2 mg.L^{-1} through membranes M_1, M_2 and M_3, respectively, for a feed concentration of 100 mg.L^{-1}. At the same TMP but different feed concentration, i.e., 400 mg.L^{-1}, the oil concentrations in the permeate were 36 mg.L^{-1}, 28 mg.L^{-1} and 11 mg.L^{-1} through membrane M_1, M_2 and M_3, respectively. This is due to the higher oil concentration of the feed; a number of small oil droplets pass more readily through the membrane. Similar behavior was also observed for other initial concentrations in the feed (Figs. 9b-9d). From the figures it may also be seen that, with an increase in concentration of oil in the field, the oil concentration in the permeate also increases at a particular TMP.

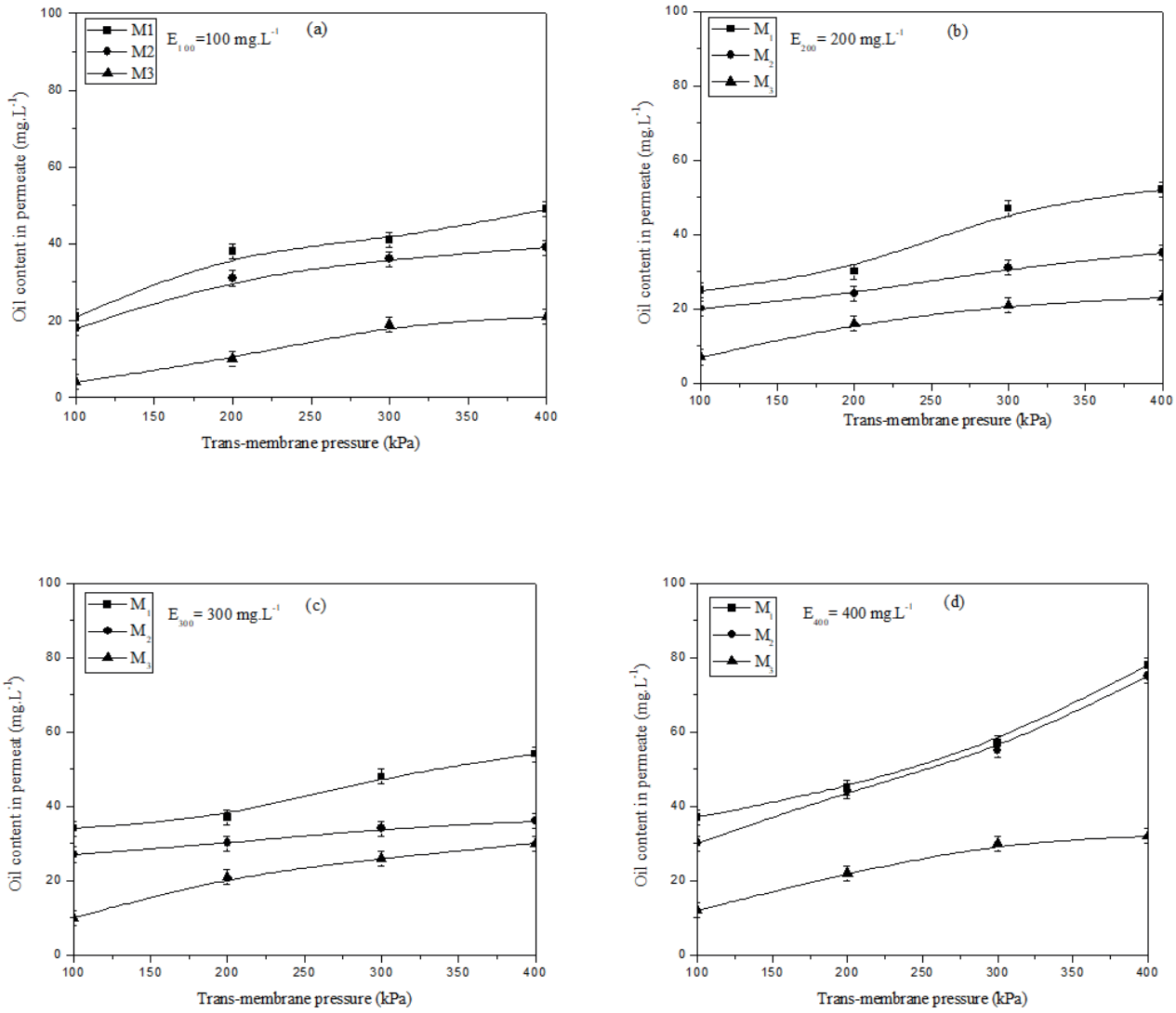

Figure 9. Oil content in the permeate after UF through membranes M_1, M_2, and M_3 of synthetic produced water (a) E_{100}: 100 mg.L^{-1} (b) E_{200}: 200 mg.L^{-1} (c) E_{300}: 300 mg.L^{-1} (d) E_{400}: 400 mg.L^{-1}.

Percentage oil rejection

The rejection of oil from the SPW is calculated as % *R* using Eq. (4) and is reported in Figs. 10a-d. From these figures it is seen that % *R* decreased with increased transmembrane pressure and % *R* increased with the increase in feed concentration. At higher oil concentrations in the synthetic produced water, the average oil droplet size is bigger than at lower oil concentration synthetic produced water; therefore, for the ultrafiltration of higher oil concentration synthetic produced water oil the rejection is greater than for low oil concentration synthetic produced water at higher trans-membrane pressure. This is due to the fact that, as the transmembrane pressure increases, the applied pressure overcomes the capillary pressure that prevents the oil from entering the membrane pores, leading to penetration of some oil droplets. At 100 kPa the percentage of oil rejection was found to be 79%, 82% and 98% through membranes M_1, M_2 and M_3, respectively, for

E_{100} = 100 mg. L^{-1}, whereas at the same transmembrane pressure the % *R* were 91 %, 93 % and 97.25 % through membranes M_1, M_2 and M_3, respectively, for E_{400} = 400 mg.L^{-1}. Therefore, despite giving a high permeate flux, this is not recommended in order to avoid oil penetration through membrane pores. As the oil concentration in the feed increased, the concentration polarization of oil near the membrane-water interface increased. As a result, oil will try to pass through the membrane pores at an increased rate, resulting in an increase in the oil concentration in the permeate. The maximum oil rejection is found to be 98% with the membrane M_3 for a feed concentration of 100 mg.L^{-1} at TMP 100kPa.

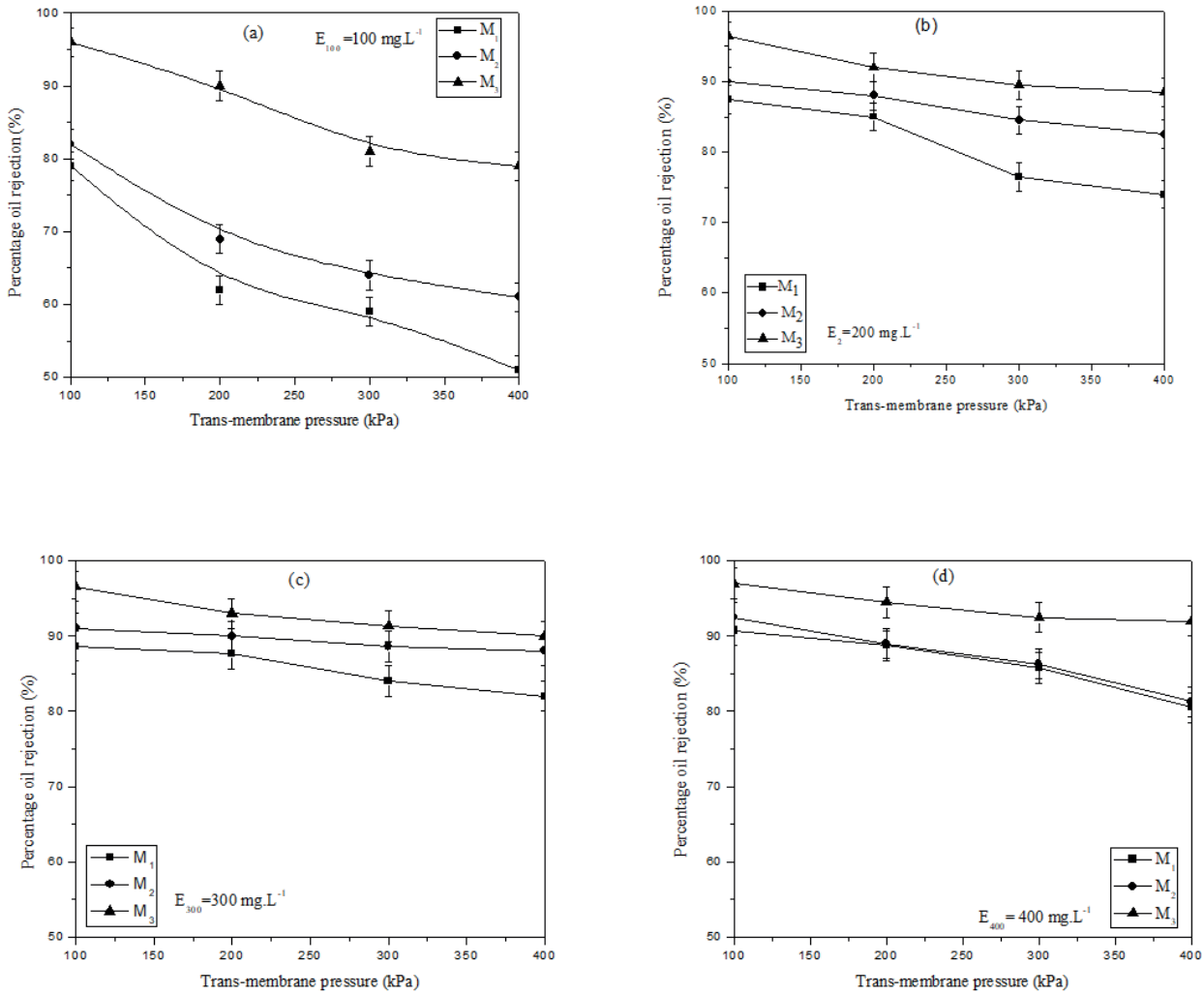

Figure 10. Percentage oil rejection through membranes M_1, $M_2$and M_3 of synthetic produced water (a) E_1: 100 mg.L^{-1} (b) E_2: 200 mg.L^{-1} (c) E_3: 300 mg.L^{-1} and (d) E_4: 400 mg.L^{-1}.

Flux decline

The permeate flux of different membranes with respect to filtration time was calculated using Eq. 3. The flux after a regular interval of 5 minutes was noted at 100 kPa trans-membrane pressure and the details of flux variation with time using M_1, M_2 and M_3 membranes are shown in Fig. 11. It was observed from these figures that the permeate flux variation using produced water is similar to pure water flux characteristics and it decreased rapidly during the first 10 minutes due to oil droplet adsorption at the membrane surface and pores. The permeate flux patterns exhibited by M_3 membranes decreased more slowly than those exhibited by M_1 and M_2 membranes; this is due to oil droplets blocking the pores more in membranes that have a large number of pores.

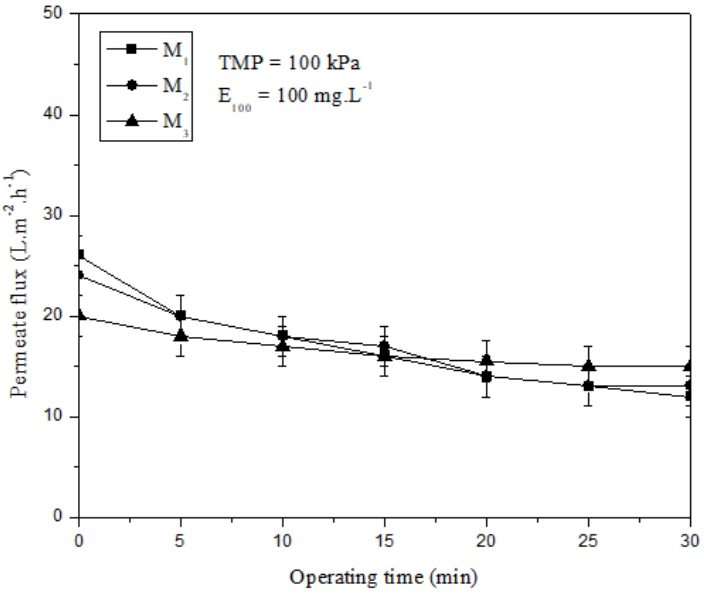

Figure 11. Flux decline through membrane M_1, M_2 and M_3 of synthetic produced water E_1: 100 mg.L^{-1} at 100 kPa.

CONCLUSIONS

In this work, the separation of oil from produced water with PSf membranes using a semi-batch cell has been performed. The effect of increasing PSf composition of membranes on permeates flux and oil rejections has been investigated in detail. Also, the paper reported the effect of TMP and feed concentration on membrane performance. The results of this study may be summarized as follows:

1 - For a particular TMP the permeate flux is found to be greater with the more porous membrane. The TMP at which the permeate flux and oil rejection are optimal is found to be 100 kPa for all three types of membranes.

2 - The pores size as well as pore area per unit surface area (porosity) of the prepared membrane is found to decrease when the PSf composition increases.

3 - The maximum rejection was found to be 98% with membrane M_3 when the oil concentration in the emulsion was 100 mg.L^{-1} at 100kpa.

4 - A significant increase in rejection and consequently a decrease in flux is observed in oil separation when the polymer composition increases.

ACKNOWLEDGEMENTS

The authors gratefully acknowledge the financial assistance provided by the Indian Institute of Technology (ISM), Dhanbad, India (FRS (29)/2010-2011/PE), to the Department of Petroleum Engineering. Thanks are also extended to all individuals associated with the project.

NOMENCLATURE

A	Membrane area (m^2)
c_f	Oil concentration in feed (mgL^{-1})
c_p	Oil concentration in permeate (mgL^{-1})
J_p	Permeate flux (Lm^{-2}h^{-1})
L	Membrane thickness (m)
P	Trans-membrane pressure (Pa)
R	Oil rejection (%)
t	Time of filtration (h)
V_p	Volume of permeate collected (L)
w_0	Weight of wet membrane (kg)
w_1	Weight of dry membrane (kg)
PSf	Polysulfone
PVP	poly(vinyl pyrrolidone)
SPW	Synthetic produced water
EWC	Equlibrium water content
FESEM	Field Emission Scanning Electron Microscopy
AFM	Atomic Force Microscopy
Greek symbols	
Δ	Difference
φ	Membrane porosity (%)
ρ_w	Density of water (kg m^{-3})

REFERENCES

Bhattacharjee S., Bhattacharya P. K., Flux decline behavior with low molecular weight solutes during ultrafiltration in an unstirred cell. Journal of Membrane Science, 72, p. 149 (1992).

Chakrabarty B., Ghoshal A. K.,Purkait M. K., Ultrafiltration of oil-in-water emulsion: Analysis of fouling mechanism. Membrane Water Treatment, 1, p. 297 (2010).

Chen G., He G., Separation of water and oil from water-in-oil emulsion by freeze/thaw method. Separation and Purification Technology, 31, p. 83 (2003).

Duong P. H. H., Chung T., Application of thin film composite membranes withforward osmosis technology for the separation of emulsified oil-water. Journal of Membrane Science, 452, p. 117 (2014).

Ghosh D., Medhi C. R., Purkait M. K., Treatment of Drinking Water Containing Iron Using Electrocoagulation. International Journal of Environmental Engineering, 2, p. 212 (2010).

Hlavacek M., Break-up of oil-in-water emulsions induced by permeation through a microfiltration membrane. Journal of Membrane Science, 102, p. 1 (1995).

Karhu M., Leiviska T., TanskanenJ.,Enhanced DAF in breaking up oil-in-water emulsions. Separation and Purification Technology, 122, p. 231 (2014).

Kumar S., GuriaC. and Mandal A.,Synthesis, characterization and performance studies of polysulfone/bentonite nanoparticles mixed-matrix ultra-filtration membranes using oil field produced water. Separation and Purification Technology, 150, p.145 (2015).

Mahendran R., Malaisamy R., Mohan D. R., Cellulose acetate and polyethersulfone blend ultrafiltration membrane part 1: preparation and characterizations. Polymer Advanced Technology, 15, p. 149 (2004).

Mandal, A.,Ojha, K. and Ghosh, D. N.,Removal of Color from Distillery Wastewater by Different Processes,Indian Chemical Engineer, 45, p264 (2003).

Mohammadi T., Kazemimoghadam M., Saadabadi, M., Modeling of membrane fouling and flux decline in reverse osmosis during separation of oil in water emulsion. Desalination, 157, p. 369 (2003).

Mondal S., Wickramasinghe S.R.,Produced water treatment by nanofiltration and reverse osmosis membranes. Journal of Membrane Science, 322, p. 162 (2008).

Nandi B. K., Das B., Uppaluri R., Purkait M. K., Studies on submicron range microfiltration inorganic membranes: Preparation. Characterization. Membrane Water Treatment, 1, (2010).

Nandi B. K., Das B., Uppaluri R., Purkait M. K., Ultrafiltration of Mosambi Juice using Low Cost Ceramic Membrane. Journal of Food Engineering, 95, p. 597 (2009).

Nandi B. K., Uppaluri R., Purkait M.K.,Microfiltration of Stable Oil-in-water Emulsions using Kaolin based Ceramic Membrane and Evaluation of Fouling Mechanism. Desalination and Water Treatment, 22, p. 133 (2010).

Padaki, M., Surya Murali, R., Abdullah, M.S., Misdan, N., A. Moslehyani, M.A. Kassim, N. Hilal, A.F. Ismail Membrane technology enhancement in oil–water separation, Desalination, 357, p. 197 (2015).

Sahoo B. K., De S., Carsky M., Enhancement of Rheological Behavior of Indian High Ash Coal−Water Suspension by Using Microwave Pretreatment. Industrial Engineering Chemistry Research, 49, p. 3015 (2010).

Samanta A., Ojha K., Sarkar A., Mandal A.,Mobility Control and Enhanced Oil Recovery using Partially Hydrolyzed Polyacrylamide (PHPA).International Journal of Oil, Gas and Coal Technology, 6, (2013).

Sarkar B. and De S., Electric field enhanced gel controlled cross-flow ultrafiltration under turbulent flow conditions. Separation and Purification Technology,74, p. 73 (2010).

Sarkar B. and De S., Prediction of permeates flux for turbulent flow in cross flow electric field assisted ultrafiltration. Journal of Membrane Science, 369, p. 77 (2011).

Singh V., Purkait M. K., Das C., Cross flow Ultrafiltration of Industrial Oily Wastewater: Experimental and Theoretical Consideration.Separation and Purification Technology, 46, p. 1213 (2011).

Sinha M. K., Purkait M.K.,Increase in hydrophilicity of polysulfone membrane using polyethylene glycol methyl ether. Journal of Membrane Science, 437, p. 7 (2013).

Vatanpour V., Madaeni S. S., Moradian R., Zinadini S., Astinchap B., Fabrication and characterization of novel antifouling nanofiltration membrane prepared from oxidized multiwalled carbon nanotube/ polyethersulfonenanocomposite. Journal of Membrane Science, 375, p. 284 (2011).

Wei-Kang Qi, Zhong-Chen Yu, Yu-Yu Liu, Yu-You Li., Removal of emulsion oil from oilfield ASP wastewater by internal circulation flotation and kinetic models. Chemical Engineering Science, 91, p. 122 (2013).